

Kinetic thermal ions effects on Alfvénic fluctuations in tokamak plasmas

X. Wang 1), S. Briguglio 2), G. Fogaccia 2), G. Vlad 2), C. Di Troia 2), F. Zonca 2),1), L. Chen 1),3), A. Bierwage 4), and H. Zhang 5),3)

1) Institute for Fusion Theory and Simulation, Zhejiang University, Hangzhou, P.R.China

2) Associazione Euratom-ENEA sulla Fusione, C.P. 65 - I-00044 Frascati, Rome, Italy

3) Department of Physics and Astronomy, University of California, Irvine CA 92697-4575, U.S.A.

4) Naka Fusion Institute, Japan Atomic Energy Agency, Ibaraki, 311-0193 Japan

5) Fusion simulation center, Peking University, Beijing 100871, P.R.China

e-mail contact of main author: wangxinnku@zju.edu.cn

Abstract. Adopting the theoretical framework for the generalized fishbone-like dispersion relation, an extended hybrid magnetohydrodynamics gyrokinetic simulation model has been derived analytically by taking into account both thermal ion compressibility and diamagnetic effects in addition to energetic particles kinetic behaviors. The extended model has been used for implementing an eXtended version of Hybrid Magnetohydrodynamics Gyrokinetic Code (XHMGC) to study thermal ion kinetic effects on Alfvénic modes driven by energetic particles, such as kinetic beta induced Alfvén eigenmode in tokamak fusion plasmas. It is shown, both analytically and by numerical simulations, that, in the presence of thermal ion kinetic effects, the beta induced Alfvén eigenmode (BAE) - shear Alfvén wave continuous spectrum can be discretized into radially trapped eigenstates known as kinetic BAE (KBAE). While the thermal ion compressibility gives rise to finite BAE accumulation point frequency, the discretization occurs via the finite Larmor radius and finite orbit width effects. Simulations and analytical theories agree both qualitatively and quantitatively. Simulations also demonstrate that KBAE can be readily excited by the finite radial gradients of energetic particle profiles.

In this work, we extend the hybrid magnetohydrodynamics (MHD)-gyrokinetic model, derived originally in [1] for applications to numerical simulations of energetic particles (EPs) driven Alfvén modes. The main differences with respect to the usual pressure coupling equation [1] are due to renormalization of the inertia term, to properly account for finite thermal ion diamagnetic effects, as well as to the gyrokinetic treatment of the thermal ion pressure tensor, which allows us to properly handle wave-particle resonant interactions in the low frequency regime, where they can be of crucial importance for the analysis of linear and nonlinear behaviors of collisionless burning plasmas. The extended model has been developed assuming ideal Ohm's law as well as ignoring finite Larmor radius (FLR) effects of thermal ions in order to simplify the technical complications while still maintaining all essential physics ingredients [2]. In practice, maintaining the ideal MHD Ohm's law as limiting case implies assuming $T_e \ll T_i$ and neglecting ion FLR effects, although finite magnetic drift orbit widths are fully retained. For demonstrating the validity of the modified equations, we show that they are equivalent to the quasi-neutrality and vorticity equations derived in [2] for the frequency range from the kinetic ballooning mode (KBM) and BAE to the toroidal Alfvén eigenmode (TAE). The extended model has been used for implementing an eXtended version of HMGC [3] Code (XHMGC) [4]. Thus, XHMGC [4] has the capability of investigating thermal ion kinetic effects on Alfvénic modes driven by energetic particles, such as kinetic beta induced Alfvén eigenmode in tokamak fusion plasmas. Meanwhile, we demonstrate the existence of KBAE [5] based on the theoretical framework presented in [6]. Both initial value problem by prescribing the initial perturbations, as well as driven resonant-cavity problem via "internal antenna" [7] excitations have been adopted to investigate KBAE properties. Numerical simulation results are also used to illustrate KBAE peculiar features with and without EP drive.

1. The extended hybrid model

Reference [2] presents a general theoretical framework for stability analyses of various modes and the respective governing equations. It shows that all modes of the shear Alfvén branch, having two scale radial structures, corresponding to the continuous spectrum, and frequencies in the range between the thermal ion transit and Alfvén frequency can be consistently described by one single general fishbone-like dispersion relation (GFLDR) [2, 8, 9, 10]. The governing equations for describing the excitation of the shear Alfvén wave (SAW) frequency spectrum by energetic ions precession, precession-bounce and transit resonances in the range $\omega_{*pi} \approx \omega_{ti} \leq \omega \leq \omega_A$, covering the entire frequency range from KBM/BAE [11, 12, 13, 14] to TAE [15, 16, 17], are generalized kinetic vorticity equation and quasi-neutrality condition, which can be written as follows (see Eq.(16) and Eq.(17) in Ref. [2]):

$$\mathbf{B} \cdot \nabla \left(\frac{k_{\perp}^2}{k_{\theta}^2 B^2} \mathbf{B} \cdot \nabla \delta\psi \right) + \frac{\omega(\omega - \omega_{*pi})}{v_A^2} \frac{k_{\perp}^2}{k_{\theta}^2} \delta\phi - \left\langle \sum_{s \neq e} \frac{4\pi e_s}{k_{\theta}^2 c^2} J_0(k_{\perp} \rho_s) \omega \hat{\omega}_{ds} \delta K_s \right\rangle + \sum_s \frac{4\pi}{k_{\theta}^2 B^2} \mathbf{k} \times \mathbf{b} \cdot \nabla (P_{\perp s} + P_{\parallel s}) \Omega_{\kappa} \delta\psi = 0, \quad (1)$$

$$\left\langle \sum_{s \neq E} \frac{e_s^2}{m_s} \frac{\partial F_{0s}}{\partial \varepsilon} \right\rangle (\delta\phi - \delta\psi) + \sum_{s=i} \langle \delta K_s \rangle = 0, \quad (2)$$

where the non-adiabatic particle response, δK_s , is obtained via the gyrokinetic equation

$$\begin{aligned} & [\omega_{tr} \partial_{\theta} - i(\omega - \hat{\omega}_d)]_s \delta K_s = i \left(\frac{e}{m} \right)_s Q F_{0s} [J_0(k_{\perp} \rho_s) (\delta\phi - \delta\psi) \\ & + \left(\frac{\hat{\omega}_d}{\omega} \right) J_0(k_{\perp} \rho_s) \delta\psi - 4\pi m_E \frac{m_s}{e_s} \frac{2J_1(k_{\perp} \rho_s)}{k_{\perp} \rho_s} \mu \left\langle \frac{2J_1(k_{\perp} \rho_s)}{k_{\perp} \rho_s} \mu \delta K_E \right\rangle]. \end{aligned} \quad (3)$$

Here, s denotes all particle species (e = bulk electrons, i = bulk ions, E = energetic particles), e_s and m_s are the species electric charge and mass, F_{0s} is the equilibrium distribution function, $\varepsilon = v^2/2$ the energy per unit mass, $\mathbf{k} \equiv -i\nabla$ is the wave vector, J_0 is the Bessel function of order zero, k_{\perp} is the perpendicular wave vector, $\rho_s^2 = v_{\perp}^2/\omega_{cs}^2$ with $\omega_{cs} = e_s B/m_s c$ being the cyclotron frequency, $\omega_{*pi} = (\mathbf{k} \times \mathbf{b} \cdot \nabla P_i)/n_i m_i \omega_{ci}$ is the thermal ion diamagnetic frequency, P_{\perp} and P_{\parallel} are, respectively, the total perpendicular and parallel plasma pressures, $\hat{\omega}_{ds} = (m_s c/e_s)(\mu + v_{\parallel}^2/B)\Omega_k$ with $\Omega_k = \mathbf{k} \times \mathbf{b} \cdot \kappa$, and $\kappa = \mathbf{b} \cdot \nabla \mathbf{b}$. Note that the difference between $\hat{\omega}_{ds}$ and $\omega_{ds} = (m_s c/e_s)(\mu \Omega_B + v_{\parallel}^2 \Omega_k/B)$, with $\Omega_b = \mathbf{k} \times \mathbf{b} \cdot \nabla B/B$, has been discussed in [2, 18] and, generally, must be handled properly. Although for many applications in low pressure ($\beta = 8\pi P/B^2 \ll 1$) plasmas, one can consider $\omega_{ds} = \hat{\omega}_{ds}$ after solving for δB_{\parallel} from perpendicular pressure balance, as implicitly assumed in equations (1)-(3) [2]. In the high frequency case, $\omega_A \geq \omega \geq \omega_{*pi} \gg \omega_{ti}$, the thermal ion non-adiabatic response δK_i can be neglected. Thus, the quasi-neutrality condition, equation (2), reduces to the ideal MHD approximation, $\delta\phi \simeq \delta\psi$; i.e. $\delta E_{\parallel} \simeq 0$ [18]. Meanwhile, neglecting the $\propto \omega_{*pi}$ term, equation (1) becomes equivalent to equation (3) in [1], i.e. the following pressure coupling equation in the hybrid MHD-gyrokinetic approach

$$\rho_b \frac{d\mathbf{v}_b}{dt} = -\nabla P_b - (\nabla \cdot \mathbf{P}_E)_{\perp} + \frac{\mathbf{J} \times \mathbf{B}}{c}; \quad (4)$$

where the subscript b denotes the bulk plasmas (electrons and thermal ions). Here, the EP contribution to the perpendicular momentum change of the plasma has been neglected, due to $n_E/n_b \ll |\omega/\omega_{*E}|$ [1, 2].

In order to extend the hybrid model to the low-frequency regime where $\omega \sim \omega_{ti}$, we need to include the effects of the thermal ion compressibility and diamagnetic drift within the hybrid simulation scheme. That is, we need to include effects associated with the δK_i terms in equation (1) and (2). The pressure coupling equation in the MHD-gyrokinetic approach, equation (4), has to be accordingly modified to

$$\rho_b \left(\frac{d}{dt} + i\omega_{*pi} \right) \mathbf{v}_b = -\nabla P_e - (\nabla \cdot \mathbf{P}_E)_\perp - (\nabla \cdot \mathbf{P}_i)_\perp + \frac{\mathbf{J} \times \mathbf{B}}{c}, \quad (5)$$

where both \mathbf{P}_E and \mathbf{P}_i need to be calculated from solutions of the gyrokinetic equations, while P_e is neglected in the present approach, assuming $T_e/T_i \rightarrow 0$.

Correspondences between equation (5) and the generalized kinetic vorticity equation, equation (1) can be established term by term [4]. The present model includes the equilibrium parallel current effects, as discussed in [2] (Appendix), and can be readily deduced from [19] as well as the modified momentum balance equation implemented in XHMGC. The present model is valid in the nonlinear case too. This is deduced easily from the comparison with the corresponding discussion from [19] and from the structures of equation (5) in the reference [20]. That equation clearly shows that, for the small FLR limit, the structure is the same as that of equation (5), since the nonlinear terms, treated explicitly, are those that are coming from convective nonlinearity and from the Maxwell stress nonlinearity, both of which are included in XHMGC.

2. Linear Dispersion Relation of KBAE

With the inclusion of small but finite FLR and FOW effects, we combine the vorticity equation (see equation (7) in [6]) and the quasi-neutrality condition (see equation (8) in [6]) and obtain [5]

$$\begin{aligned} \left(1 + \left(1 - \frac{\omega_{BAE}^2}{\omega^2} \right) \tau b_i \right) \partial_\theta^2 \delta\Phi + \frac{\omega^2}{\omega_A^2} \left(1 - \frac{3}{4} b_i \right) \delta\Phi \\ - \frac{\omega_{BAE}^2}{\omega_A^2} \left(1 + q^2 \frac{\omega \omega_{ti}}{\omega_{BAE}^2} S(\omega) b_i \right) \delta\Phi = 0, \end{aligned} \quad (6)$$

where $\omega_A \equiv v_A/qR_0$ is the Alfvén frequency, $v_A = B/\sqrt{4\pi n_i m_i}$, $\omega_{ti} = \sqrt{2T_i/m_i}/qR_0$, $\tau = T_e/T_i$, and $b_i \equiv k_\perp^2 \rho_{Li}^2$ with $\rho_{Li}^2 = T_i m_i c^2 / e_i^2 B^2$, $\omega_{BAE} = q\omega_{ti}(7/4 + \tau)^{1/2}$ is defined as the value of the asymptotic (high-frequency limit) BAE frequency. Here, the first term on the LHS contains τb_i term due to the usual electron pressure corrections to the ideal Ohm's law, which is negligible near the BAE accumulation point, as discussed in [6, 21]. The second term includes the thermal ion FLR correction to the charge density due to the polarization current; while the third term contains the thermal ion FOW corrections to the charge density due to the perturbed diamagnetic current. Note that it is this latter term that accounts for peculiar features associated with geodesic curvature in toroidal geometry [6, 21]. The FLR/FOW correction is important when one considers mode conversion due to radial singular structures associated with resonant excitation of the SAW continuous spectrum. Equation (3) reduces to the well known result for kinetic Alfvén waves (KAW) [22, 23] by taking the limit $\omega_{BAE}/\omega \rightarrow 0$. We can cast equation (6) into the following standard form

$$\partial_\theta^2 \delta\Phi + \Lambda^2 \delta\Phi - \theta^2 Q^2(\omega) \delta\Phi = 0; \quad (7)$$

where $\Lambda^2 = (qR_0 k_\parallel)^2 = (\omega^2 - \omega_{BAE}^2)/\omega_A^2$ gives the local dispersion relation [24] and

$$Q^2(\omega) = s^2 k_\theta^2 \rho_{Li}^2 \frac{\omega^2}{\omega_A^2} \left[\frac{3}{4} + q^2 \frac{\omega_{ti}}{\omega} S(\omega) + \frac{\tau (\Lambda \omega_A / \omega)^4}{1 + \tau \omega_{*ni} / \omega} \right]. \quad (8)$$

In this work, when comparing numerical simulation results with analytical theory, we further consider the limit $\tau = 0$, which allows us to assume the ideal MHD Ohm's law [4]. We also neglect thermal ion FLR effects; i.e. we drop the $3/4$ factor in equation (8). From the expression of $S(\omega)$ given in [25], one can readily obtain

$$\frac{3}{4} + q^2 \frac{\omega_{ti}}{\omega} S(\omega) \simeq \frac{3}{4} - \frac{13}{7} \frac{\omega_{BAE}^2}{\omega^2} + \frac{747}{98} \frac{\omega_{BAE}^4}{\omega^4} + i\pi^{1/2} q^4 e^{-\omega^2/4\omega_{ti}^2} (\omega^5/256\omega_{ti}^5 + \omega^3/32\omega_{ti}^3). \quad (9)$$

Note that, equation (9) represents the approximation of $(3/4 + q^2\omega_{ti}/\omega S(\omega))$ under the condition $(7/4 + \tau)q^2 \gg 1$. In this case, $Re[3/4 + q^2\omega^2/\omega_{ti}S(\omega)] > 0$ is always satisfied. Meanwhile, as discussed in [25], the sign of $Re[3/4 + q^2\omega^2/\omega_{ti}S(\omega)]$ can change at low frequency with possible interesting implications on the mode dynamics. Equation (4) can be solved locally for the

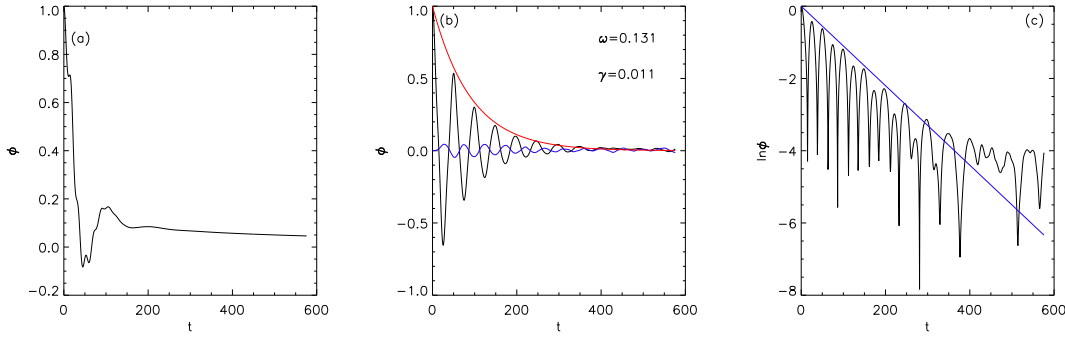


FIG. 1. : Time history of the normalized electrostatic potential at the accumulation point, (a) without kinetic thermal ions; (b) with kinetic thermal ions for $\beta_{ic} = 0.0072$, where the black line is the real part of the electrostatic potential; the blue line is the imaginary part; and the red line corresponds to an exponentially scaling $e^{-\gamma t}$; (c) $|\phi|$ in log scale.

discretized KBAE spectrum near the BAE accumulation point. The existence of radially localized discrete modes can be understood as follows: the KAW is trapped within the potential well formed on the “high frequency side” of the local SAW continuous spectrum [22, 23] and modified by thermal ion compressibility effects near the BAE accumulation point. Meanwhile, on the “low frequency side” [22, 23], KAW is evanescent. In this condition, analogous to that discussed by Rosenbluth and Rutherford for KAW in [26] and Mett and Mahajan for kinetic toroidal Alfvén Eigenmode (KTAE) in [27], radially bound states (discrete modes) can exist, whose energy levels correspond to those of the “harmonic oscillator” described by equation (7).

$$\Lambda^2 = (2\ell + 1)Q \quad (10)$$

with $\ell = 0, 1, 2, \dots$ being the “radial quantum number” [6, 21]. Note that (10) describes the energy levels of well localized radially bound states. The finite coupling to the (radial) external region (ideal region) and non-uniform plasma response via longer wavelength feature of the global mode structures is described by [6, 21, 28]

$$-2Q^{1/2} \frac{\Gamma(3/4 - \Lambda^2/4Q)}{\Gamma(1/4 - \Lambda^2/4Q)} = \delta W_f + \delta W_k. \quad (11)$$

Here, δW_f and δW_k are, respectively, the perturbed potential energies of the background MHD fluid and EP in the ideal region. Equation (8) reduces to the generalized fishbone like dispersion relation [2, 21, 29]

$$i\Lambda = \delta W_f + \delta W_k \quad (12)$$

in the limit $|\Lambda^2/4Q| \gg 1$; i.e. when the fine structures of “discretized” SAW continuous spectrum are unimportant due to the intrinsic (linear) frequency line width connected with EP drive or time coherence of the external source [10, 25, 30]. This can be easily verified by taking the large argument expansion of the Euler gamma functions. Global plasma properties, thus, affect the BAE/KBAE dispersion relations [6, 21, 28, 29] via δW_f and δW_k . It is worthwhile noting that, for most unstable modes that are relevant for the description of EP transport in burning plasmas [2, 29, 31], EP dynamics enter only via δW_k and never contribute to the inertial layer. The dispersion relation for radially localized KBAE modes, equation (10), is readily obtained from equation (11) for either $|\delta W_f + \delta W_k| \ll |Q|^{1/2}$ (even modes, $\ell = 0, 2, 4 \dots$) or $|\delta W_f + \delta W_k| \gg |Q|^{1/2}$ (odd modes, $\ell = 1, 3, 5 \dots$).

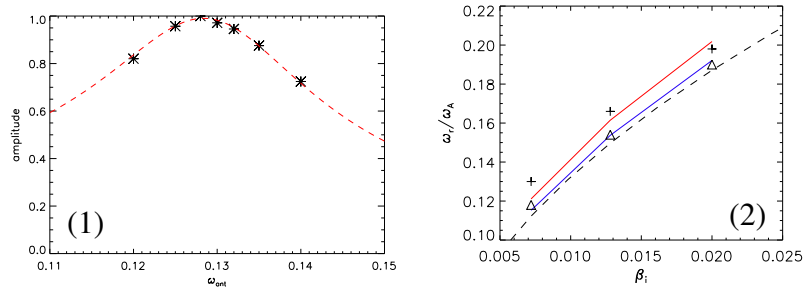


FIG. 2. : (1) Maximum amplitude for different antenna frequency. * is the amplitude (a.u.); red dashed line corresponds to the fitting function given in equation (13). (2) Frequency comparison between numerical simulation results by “antenna” excitations and theoretical values. Δ is eigenfrequency from simulations for $n=1$, + is eigenfrequency from simulations for $n=3$, the black dashed line is ω_{BAE} the accumulation point frequency, the blue line is KBAE frequency for $n=1$, and the red line is KBAE frequency for $n=3$.

3. Simulation Results

Both initial perturbations and “antenna” excitations have been used to simulate BAE or KBAE with kinetic thermal ion dynamics. Simulations refer to an equilibrium magnetic field characterized by shifted circular magnetic surfaces with inverse aspect ratio $a/R_0 = 0.1$ and the q -profile given, in the cylindrical approximation, by $q(r/a) = q(0) + [q(a) - q(0)]r^2/a^2$, with $q(0) = 2.7$ and $q(a) = 3.9$. In the initial-value simulations, $n = 3$ and $m = 9$ perturbation in the electrostatic potential is initially introduced around the $q = 3$ location. In the present simulations, the equilibrium thermal ion density and temperature are kept uniform to neglect the diamagnetic drift. Figure 1 (a) and (b) show the time histories of the electrostatic potentials without and with thermal ions kinetic effects respectively. Figure 1 (a) shows that, in the case without thermal ions kinetic effects, the perturbed field is purely damped due to phase mixing at the accumulation point, where the accumulation point frequency is $\omega_{acp} = 0$. When thermal ion kinetic effects are taken into account, figure 1 (b) shows that the perturbed field oscillates with a finite frequency and damps exponentially due to the ion Landau damping, as demonstrated from the semi-log plot shown in figure 1 (c). The simulation shown in figure 1

(b) and (c) refer to $\beta_{ic} = 0.0072$. Here, β_{ic} is defined as $\beta_{ic} = 8\pi n_{ic} T_{ic} / B^2$, and the subscript ic denotes core ions.

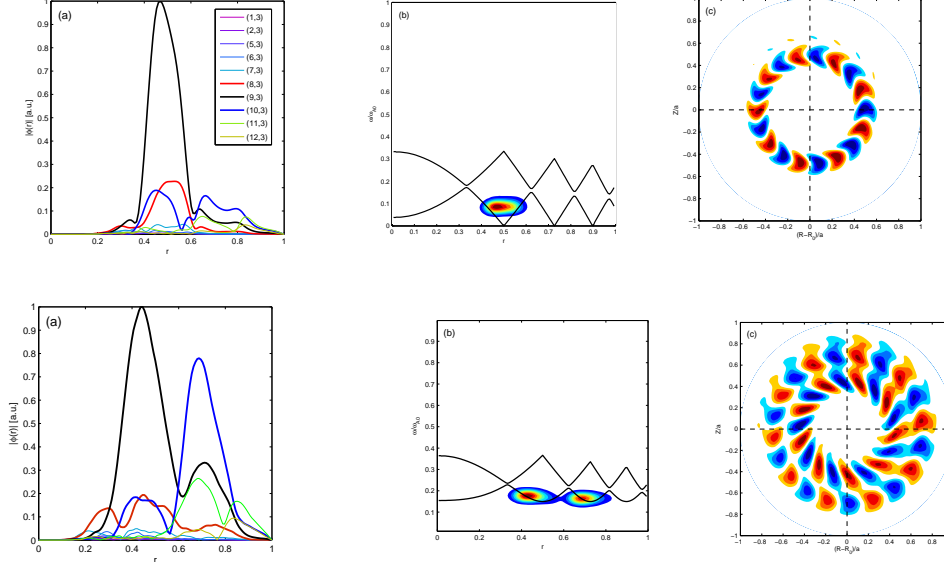


FIG. 3. : Simulation results of mode excitations by EP for $\beta_H = 0.009$. The top panels describe the case without kinetic thermal ions, the bottom panels describe the case with kinetic thermal ions for $\beta_{ic} = 0.0128$. Column (a) is the radial mode structure, column (b) is the frequency spectrum and column (c) is the poloidal mode structure contour plot.

We then use “antenna” excitation [19] to investigate the eigenmode frequencies, damping rate and the mode structures. In figure 2 (1), for different “antenna” frequencies, the maximum amplitudes of the electrostatic potential response are plotted at $r = 0.5a$. The damping rate is related to the maximum wave response amplitude by [32]

$$\delta\phi_{max} \propto \frac{1}{\sqrt{(\omega_0^2 - \omega_{ant}^2) + 4\gamma^2\omega_{ant}^2}}. \quad (13)$$

Here, $\delta\phi_{max}$ is the maximum amplitude, ω_{ant} is the “antenna” frequency, $\omega_0^2 = \omega_r^2 + \gamma^2$, ω_r is the eigenmode real frequency given by the frequency corresponding to the maximum $\delta\phi_{max}$ and γ is the damping rate. Thus, the eigenmode frequency and damping rate can be measured. In figure 2 (2), we have plotted the BAE accumulation frequencies ω_{BAE} in the fluid limit, analytically predicted $\ell = 0$ KBAE eigenmode frequencies from equation (10), as well as eigenmode frequencies determined via “antenna” excitation simulations versus β_i for $n = 1$ and $n = 3$, respectively. Note that the analytically predicted KBAE frequencies are in good agreement with those obtained from numerical simulation results; and both are higher than the ω_{BAE} accumulation frequencies. In addition, in numerical simulations, the observed oscillation frequencies are constant across the mode radial extension; further indicating the oscillations are eigenmodes. Note also that the $n = 3$ KBAE frequency is higher than the $n = 1$ KBAE frequency; consistent with the theoretical predictions of equation (10) and that the (FLR)FOW kinetic effects increase with the toroidal mode number, n . There is no observation of the higher ($\ell \geq 1$) radial eigenstates of KBAE. This may be the case either because the potential well is not sufficiently deep to trap the higher eigenstates [6] or due to the relatively strong damping,

the frequency resolution is not sufficiently fine to resolve the neighboring eigenstates. The simulation results is verified through benchmarks with GTC [34].

Simulation results of Alfvénic modes excited by EPs are shown in figure 3. Simulations refer to a fixed value of $\beta_H = 8\pi n_H m_H v_H^2 / B^2 = 0.009$ (the on axis EP pressure parameter) and toroidal mode number $n=3$. The EP velocity-space equilibrium distribution function is taken to be purely circulating slowing-down distribution [33] with birth energy $E_0 = m_H v_H^2$, where $m_H = m_{ic}$. The on-axis parameters are: $n_{H0}/n_{ic} = 0.05$, $v_H/v_A = 0.3$, $\rho_{LH}/a = 0.03$. The EP equilibrium density profile is taken to be $n_H(r) = n_{H0}(1 + 2(r/a)^3 - 3(r/a)^2)$. The

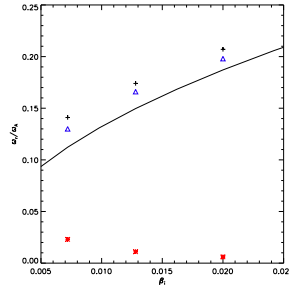


FIG. 4. : The real frequency and growth rate for the $n=3$ mode versus different thermal ion pressure parameters for $\beta_{ic} = 0.0072, 0.0128, 0.02$. “+” is the mode real frequency of simulation results by EP excitations; “ \triangle ” is the KBAE frequencies by antenna excitations; solid line denotes the theoretical BAE accumulation point frequency; red “*” is the growth rate by EP excitation simulations.

top panels describe excitations without thermal ion kinetic effects. Simulation results with kinetic thermal ion effects are presented in the lower panels. Column (a) of the top panel shows that the excited mode is localized around $r = 0.5$, where the EP drive is maximum and, correspondingly, the dominant poloidal mode number is $m = nq = 9$. Meanwhile, column (b) shows that the real frequency of the mode is around $0.85\omega_{tE}$, where $\omega_{tE} = v_H/qR$ is the beam-ion transit frequency at $q = 3$. These simulation results are, thus, consistent with the theoretical predictions for the energetic particle mode (EPM) [9, 13]. Note that EPM exists entirely due to EPs; such that its radial localization, real frequency and linear growth rate are intrinsically determined by the EP pressure gradient drive, characteristic dynamical frequencies and competition between the EP-wave resonance drive and the BAE-SAW continuum damping. When thermal ion kinetic effects are included, column (b) of the lower panels in figure 3 shows that the SAW continuum has accumulation points at the finite BAE frequencies. Meanwhile, the excited modes, as shown in column (a) and (b), are localized around $r \approx 0.5a$ and $r \approx 0.7a$ corresponding, respectively, to the dominant poloidal harmonics $m = 9$ and $m = 10$. Note that, from column (b), both modes have frequencies above BAE accumulation point; i.e., in the range of KBAE. That the $m=9$ mode has an intensity higher than that of $m=10$ is due to the stronger EP drive around $r = 0.5a$. We emphasize that, with thermal ion kinetic effects included, there exists the frequency gap with accumulation point frequency at ω_{BAE} ; which either nullifies or significantly reduces the continuum damping rate. This explains why the weakly driven $m = 10$ mode is absent in the top panels without the kinetic thermal ion gap. That EP excited oscillations are KBAE is further demonstrated in figure 4; where the real frequencies of simulation results by both “antenna” excitations and EP excitations are plotted versus the thermal ion temperature. Figure 4 clearly shows that the frequencies scale properly with the BAE frequency. That the growth rate decrease with the thermal ion temperature can be understood as due to either the stronger damping and/or the weaker EP driven with the higher BAE frequency.

Acknowledgments We acknowledge useful discussions with Z. Lin. This work is supported by the Euratom Communities under the contract of Association between EURATOM/ENEA, USDOE GRANTS, SciDAC, GSEP and China Special Project for ITER (2009GB105005).

References

- [1] PARK, W., et al., Phys. Fluids B **4** (1992) 2033.
- [2] ZONCA, F., and CHEN, L., Plasma Phys. Control. Fusion **48** (2006) 537.
- [3] BRIGUGLIO, S., et al., Phys. Plasmas **2** (1995) 3711
- [4] WANG, X., et al., 2010 An extended hybrid MHD-Gyrokinetic model for numerical simulation of shear Alfvén waves in burning plasmas *to be submitted to Phys. Plasmas*
- [5] WANG, X., ZONCA, F., and CHEN L., (2010) for publication by Plasma Phys. Control. Fusion
- [6] ZONCA, F., et al., Plasma Phys. Control. Fusion **40** (1998) 2009
- [7] CHEN, L., et al., Proc. 23rd Int. Fusion Energy Conf. (Daejon, Korea 2010) **THW/P7-05**
- [8] CHEN, L., WHITE, R. B., and ROSENBLUTH, M. N., Phys. Rev. Lett. **52** (1984) 1122
- [9] CHEN, L., Phys. Plasmas **1** (1994) 1519
- [10] CHEN, L., and ZONCA, F., Physica Scripta **1995** (1995) 81
- [11] HEIDBRINK, W. W., et al., Phys. Rev. Lett. **71** (1993) 855
- [12] TURNBULL, A. D., et al., Phys. Fluids B: Plasma Phys. **5** (1993) 2546
- [13] TSAI S. T., and CHEN, L., Phys. Fluids B: Plasma Phys. **5** (1993) 3284
- [14] BIGLARI, H., and CHEN, L., Phys. Rev. Lett. **67** (1991) 3681
- [15] CHENG, C. Z., CHEN, L., and CHANCE, M. S., Annals of Physics **161** (1985) 21
- [16] CHEN, L., Theory of Fusion Plasmas ed. Vaclavik J. et al. (Bologna:SIF) p 327
- [17] FU, G. Y., and DAM J. W. V., Phys. Fluids B **1** (1989) 1949
- [18] CHEN, L., and HASEGAWA, A., 1991 J. Geophys. Res. **96** (1991) 1503
- [19] DENG W., et al., 2010 *Gyrokinetic particle simulations of reversed shear Alfvén eigenmode excited by antenna and fast ions* accepted by Phys. Plasmas
- [20] CHEN, L., et al., Nucl. Fusion **41** (2001) 747
- [21] ZONCA, F., et al., Phys. Plasmas **6** (1999) 1917
- [22] HASEGAWA A., and CHEN, L., Phys. Rev. Lett. **35** (1975) 370
- [23] HASEGAWA, A., and CHEN, L., Phys. Fluids **19** (1976) 1924
- [24] ZONCA, F., et al., Plasma Phys. Control. Fusion **38** (1996) 2011
- [25] ZONCA, F., and CHEN, L., EPL **83** (2008) 35001
- [26] ROSENBLUTH, M. N., and RUTHERFORD, P. H., Phys. Rev. Lett. **34** (1975) 1428
- [27] METT, R. R., and MAHAJAN, S. M., Phys. Fluids B: Plasma Phys. **4** (1992) 2885
- [28] NGUYEN, C., et al., Phys. Plasmas **15** (2008) 112502
- [29] CHEN, L., and ZONCA, F., Nucl. Fusion **47** (2007) S727
- [30] ZONCA, F., and CHEN, L., Phys. Plasmas **3** (1996) 323
- [31] ZONCA, F., et al., Plasma Phys. Control. Fusion **48** (2006) B15
- [32] HARRIS, J., et al., Handbook of physics (Springer: edited by Harris J. et al.) (2002)
- [33] VLAD, G., et al., Nucl. Fusion **49** (2009) 075024
- [34] ZHANG, H. S., et al., 2010 *Gyrokinetic particle simulation of beta-induced Alfvén eigenmode* accepted by Phys. Plasmas